On the Effect of 3D Wave Propagation on 2D Regional-Scale Velocity Model Building

Andrzej Górszczyk, Romain Brossier, Ludovic Métivier

▶ **To cite this version:**

Andrzej Górszczyk, Romain Brossier, Ludovic Métivier. On the Effect of 3D Wave Propagation on 2D Regional-Scale Velocity Model Building. Journal of Geophysical Research : Solid Earth, 2024, 129 (3), 10.1029/2023jb028172 . hal-04792460

HAL Id: hal-04792460
https://hal.science/hal-04792460v1

Submitted on 20 Nov 2024

HAL is a multi-disciplinary open access archive for the deposit and dissemination of scientific research documents, whether they are published or not. The documents may come from teaching and research institutions in France or abroad, or from public or private research centers.

L'archive ouverte pluridisciplinaire **HAL**, est destinée au dépôt et à la diffusion de documents scientifiques de niveau recherche, publiés ou non, émanant des établissements d'enseignement et de recherche français ou étrangers, des laboratoires publics ou privés.

JGR Solid Earth

RESEARCH ARTICLE
10.1029/2023JB028172

On the Effect of 3D Wave Propagation on 2D Regional-Scale Velocity Model Building

Andrzej Górszczyk[1,2], **Romain Brossier**[2], **and Ludovic Métivier**[2,3]

[1]Institute of Geophysics, Polish Academy of Sciences, Warsaw, Poland, [2]ISTerre, Université Grenoble Alpes, Grenoble, France, [3]Université Grenoble Alpes, CNRS, LJK, Grenoble, France

Key Points:

- 2D seismic data acquired in complex geological settings are affected by the 3D-effect, which leads to the errors during 2D seismic imaging
- Processing of the data from the 2D profiles within the 3D models can provide partial remedy to the 3D effect at the processing stage
- Robust 3D full-waveform inversion of academic crustal-scale data is possible once supported by optimization of the acquisition design

Supporting Information:

Supporting Information may be found in the online version of this article.

Correspondence to:

A. Górszczyk,
agorszczyk@igf.edu.pl

Citation:

Górszczyk, A., Brossier, R., & Métivier, L. (2024). On the effect of 3D wave propagation on 2D regional-scale velocity model building. *Journal of Geophysical Research: Solid Earth*, *129*, e2023JB028172. https://doi.org/10.1029/2023JB028172

Received 31 OCT 2023
Accepted 20 FEB 2024

Author Contributions:

Conceptualization: Andrzej Górszczyk
Data curation: Andrzej Górszczyk
Formal analysis: Andrzej Górszczyk
Funding acquisition: Andrzej Górszczyk, Romain Brossier, Ludovic Métivier
Investigation: Andrzej Górszczyk
Methodology: Andrzej Górszczyk
Project administration: Andrzej Górszczyk
Resources: Andrzej Górszczyk
Software: Andrzej Górszczyk, Romain Brossier, Ludovic Métivier
Supervision: Andrzej Górszczyk
Validation: Andrzej Górszczyk
Visualization: Andrzej Górszczyk
Writing – original draft: Andrzej Górszczyk
Writing – review & editing: Ludovic Métivier

© 2024. American Geophysical Union. All Rights Reserved.

Abstract Active seismic surveys are routinely employed by academia to study geological structure of the crust and upper mantle. Wavefields generated during these surveys are sampled at the receiver locations, but the wave-paths traveled from a source to a sensor remains unknown. Although seismic acquisition layouts designed to investigate complex crustal-scale environments are often two-dimensional, the seismogram recorded at the receiver location represents information gathered along the three-dimensional wavepaths that might offset from the 2D source/receiver profile along its transverse direction. This so-called 3D-effect distorts the results of 2D seismic imaging, which is unable to handle the out-of-plane propagation. Despite the numerous 2D seismic imaging case studies, the assessment of this issue is often overlooked. However, the problem exists - especially for crustal-scale profiles, where seismic energy propagates over distances of hundreds of kilometers and probes different crustal units. In this work we investigate the impact of 3D-effect on the results of 2D velocity model building from the academic ocean-bottom seismometer data. We show with polarization analysis how the 3D-effect can manifest itself in the data domain. Using various scenarios of acquisition we evaluate the imprint of the out-of-plane propagation on the data and the results of full-waveform inversion. We show that 2D velocity model building from the seismic profiles acquired in the complex geological setting can lead to wrong solution. Looking for the remedy to this issue we couple different configurations of acquisition geometries with 3D full-waveform inversion that allow to handle the 3D effect and provide correct model reconstruction.

Plain Language Summary Subsurface structures can often form complex geological settings. Assumption that 2D seismic surveys and 2D imaging of resulting data is sufficient to reconstruct such complex environment might often be wrong and can lead to false geological interpretation. In this study we demonstrate how the 2D seismic data acquired in a subduction zone environment can be affected with various intensity by the out-of-plane wavefield propagation and how this can bias the velocity model reconstruction. We demonstrate how this issue can manifest itself in the data domain and how it can be solved by changing the approach to the crustal-scale seismic acquisition from 2D to 3D. We show that 3D velocity model building at wavelet resolution from academic seismic data is possible nowadays with available computing power and efficient source codes. Through this work we want to promote this kind of seismic data acquisition and processing for better and less uncertain reconstructions of the key crustal-scale geological settings that shape our planet.

1. Introduction

Regional-scale active seismic surveys became over recent decades the methods of choice to probe the lithosphere (e.g., Carbonell et al., 2000; Collins et al., 1989; Corbalán et al., 2021; Fujie et al., 2016; Funck et al., 2001; Gorszczyk et al., 2019; Gómez de la Peña et al., 2020; Klingelhöfer et al., 2005; Kopp et al., 2002; McGeary & Warner, 1985; Minshull et al., 1994; Schultz & Crosson, 1996; Stern & Benson, 2011; Van Avendonk et al., 2006). This is because of their ability to generate and record redundant broadband wavefields that can be exploited with inversion methods (e.g., traveltime tomography, migration, full-waveform inversion) to build the models of subsurface at much higher resolution than it can be achieved with passive seismic or non-seismic methods. Theoretical resolution of full-waveform inversion (FWI, Tromp, 2019; Virieux & Operto, 2009) is as high as half of the inverted wavelength making it possible to reconstruct complex structural details of sub-surface - given that the multidirectional wavefield illumination is provided. This condition is, however, rarely met for academic deep crustal seismic surveys. In practice, these experiments assume compromise between the survey logistic (e.g., pool of available instruments, costs and time of shooting) and the key parameters of acquisition geometry (e.g., fold, offset and azimuth range). This compromise leads to sparse 2D acquisition geometries. In particular, marine OBS surveys are often conducted with a few tens of receivers deployed along the 2D profiles

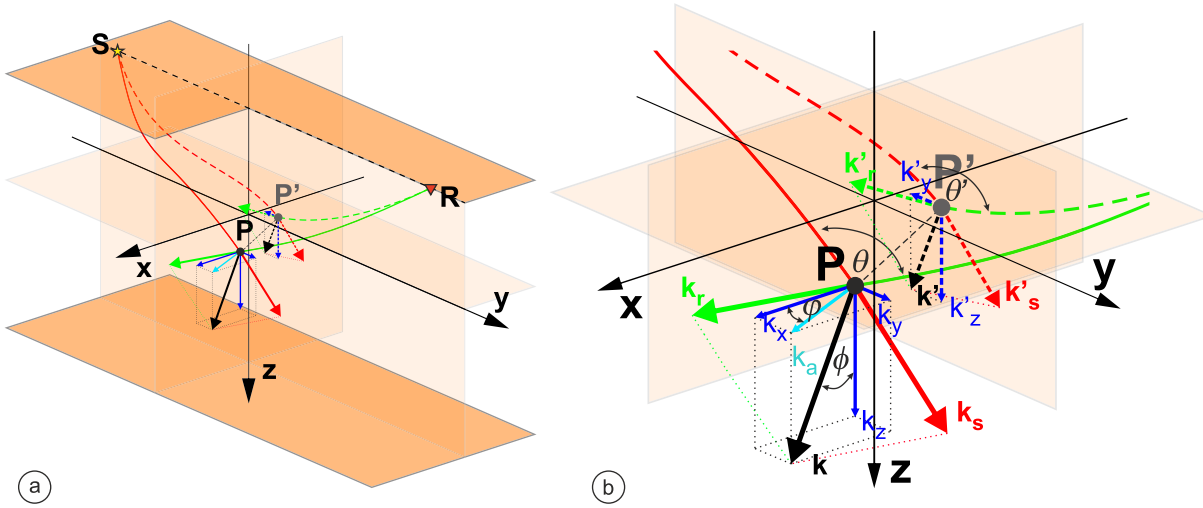

Figure 1. (a) Sketch of the single source/receiver (**S/R**) acquisition and the wavenumber vectors mapped by FWI at scattering points **P/P′**. (b) Zoom on (a). The 3D vector **k** corresponds to the true 3D **SPR** wavepath while the 2D vector **k′** is its 2D representation obtained during 2D wave modeling along 2D **SP′R** wavepath. **P′** is the projection of scattering point **P** on the vertical plane associated with the axis of the (**S/R**) profile. Local wavenumber vectors **k/k′** are sums of $\mathbf{k_s}/\mathbf{k_{\xi}}$ and $\mathbf{k_r}/\mathbf{k_{\xi}}$ vectors respectively associated with the raypaths emerging from the source **S** and receiver **R** creating the scattering angle θ/θ' at the scattering point **P/P′**. Dip and azimuth of the wavenumber vector **k** is defined by the ϕ and φ angles (adapted from Górszczyk and Operto (2021)).

that can be up to few hundreds of kilometers long (Abramovitz et al., 1997; Christeson et al., 2014; Grevemeyer et al., 2022; Janik et al., 2022). As a result the high costs of dense 3D surveys are mitigated at the price of the quality of the resulting data. This in turn limits the potential of these datasets to be fully exploited by advanced processing techniques of seismic imaging - such as wave-based migration and inversion methods (Monk, 2020). In particular, the 2D data acquisition and subsequent 2D imaging pose the inconsistency between the 3D wavepath traveled during the survey and the 2D wavepath forced during the processing. To minimize the potential impact of the 3D effect on the 2D seismic data there is a tendency (where possible) to orient the seismic profiles perpendicularly to the structural trend - assuming cylindrical shape of geological structures. However, if the 3D-effects are strong due to the complexity of the underlying setting, then the 2D assumption of wavefield propagation cannot honor the field conditions and ultimately must lead to certain errors in the reconstructed velocity model or migrated image. Consequently, further geological interpretation driven by the results of such seismic imaging is biased and leads to potentially false conclusions that might be difficult to verify if no other supporting data are available. This is especially important when the key quantitative or structural interpretation is based on the subtle changes of the reconstructed parameter.

The limitation of 2D seismic acquisition and processing has been well understood by the seismic exploration industry where nowadays the densely sampled marine (also land where possible) surveys brought the tremendous increase of the standards in seismic imaging (Operto et al., 2023; Sedova et al., 2019). Introduction of nodal systems allowed for recording long offset wide azimuth multicomponent data that opened wide range of possibilities in terms of how they can be utilized during processing (Jack, 2021). Indeed, recent decade has shown a massive development of FWI (e.g., ultra-high frequency FWI (Kalinicheva et al., 2020)) and migration methods (e.g., Reverse Time Migration—RTM and Least-Squares Reverse Time Migration–LSRTM (Zeng et al., 2014; Zhou et al., 2018)), that coupled with the leading-edge acquisition systems of multicomponent seismic data constitute nowadays a powerful technology to reconstruct the subsurface models. Perhaps one of the key obstacles that was certainly hampering this development was the suboptimal sampling of the subsurface provided by 2D surveys. This is because lithological heterogeneities cause changes in the wave propagation regime, as well as in the direction of propagation indicated at any point of subsurface **P** by the wave vector **k** that is three-dimensional (see Figure 1). The spectrum of **k** vectors spanned at each point **P** by a certain acquisition geometry translates to the resolution power of FWI (Beylkin, 1987; Miller et al., 1987; Vermeer, 2012). Intuitively, denser 2D source/receiver deployments enable fine-scale sampling of the subsurface and have the potential to probe the structure of interest from a broad range of perspectives, albeit sharing a single azimuth. In this context, Beller et al. (2018)

demonstrated in a teleseismic study that the reconstruction of a velocity model from a dense 2D acquisition geometry is actually worse than when considering a coarse 3D array of receivers. This is because an areal deployment of receivers provides the illumination of the target, which generates wider range of the scattering angles θ at various azimuths φ. This in turn translates to the broader spectrum of wavenumber vectors **k** spanned at a given point **P** to better constrain its reconstruction. The 2D acquisition geometry is therefore unable to solve the clear inconsistency between the 3D wavepath that has been taken during the field experiment and the 2D wavepath imposed during 2D processing. In Figure 1b the 2D and 3D wavepaths **SP′R** and **SPR** are different, and so are the coordinates of the points **P** and **P′**, as well as the wavenumber vectors **k′** and **k**. The scale of this inconsistency can vary from negligible to critical depending on the complexity of the media. However, one may expect that processing of seismic data from complex geological setting under 2D approximation must lead to the biased reconstruction (e.g., errors in velocity models or artifacts in the migrated image) regardless used imaging approach. In terms of regional scale seismic imaging, despite the lack of spatial sampling, low-frequency content or multiazimuthal coverage in the archival academic seismic datasets, there are documented onshore and offshore case studies that attempted to process such data with FWI and extracted useful structural information beyond the resolution-limit of the traveltime tomography (Adamczyk et al., 2015; Górszczyk et al., 2017, 2021; Kamei et al., 2013; H. Li et al., 2023; Operto et al., 2006; Ravaut et al., 2004). However, the limitations originating from the legacy acquisition design (e.g., sparse 2D deployments) made it difficult to fully exploit the potential of FWI —that is, the high-confidence multiparameter and high-resolution model reconstitution. To mitigate this issue, recently sparse 3D OBS surveys started to emerge (e.g., Boddupalli et al., 2021; Heath et al., 2019; Morgan et al., 2016) that have potential to provide multiazimuthal coverage. Despite this, further detailed optimization of these type of surveys for the purpose of academic regional-scale FWI is needed.

The purpose of this study is to evaluate the ability of 2D regional-scale FWI to handle the out-of-plane propagation within complex media and to investigate how this effect can manifest itself in the data and the final results. Through the insight into the wave propagation within the different subsurface models we want to clearly show the existence and the scale of the problem and make the first attempts to broader investigation of the optimization of regional-scale 3D academic surveys designed for high resolution subsurface model reconstruction.

Our investigations of 3D effect are based on the high-resolution GO_3D_OBS synthetic model of subduction zone (Górszczyk & Operto, 2021). This benchmark model was created to test various seismic imaging approaches at the crustal scale. From the full model we extract 3D target models in various configurations and we use those models to generate the seismic data along the 2D OBS lines (located at central inlines of the models). Subsequently, we use 2D FWI to evaluate how the out-of-plane propagation affects the results of the velocity model building when the processed data are generated within the 3D target models but extracted along the 2D receiver profiles. We compare those results with the idealized scenario where the 2D FWI is applied to the data extracted along the same 2D receiver profiles, but generated within the 2D velocity models coincident with the geometry of these profiles. We analyze the wavepaths and OBS gathers of 2D and 3D seismic data that clearly show the differences in the anatomy of the arrivals—not only in terms of the amplitude trends but also significant phase shifts. We perform polarization analysis of the multicomponent data that allows us to estimate the horizontal azimuth angle at the receiver locations and assess the scale of the 3D effect. Finally we also run 3D FWI with different OBS acquisition settings to investigate their impact on the final model reconstruction. We also present that the problem of the out of plane propagation can introduce significant errors to the input data for ray based methods like First Arrival Tomography (FAT).

In the following section we briefly introduce our FWI scheme, experimental setup and the data we use in this study. Then we describe the FWI results obtained with two different acquisition scenarios that are less and more prone to the 3D effect. We further present how polarization analysis can be helpful to identify the out-of-plane propagation in the data space and how various 3D acquisition layouts coupled with subsequent 3D FWI can solve the problem of 3D effect encountered during 2D data processing. Finally we discuss some of the practical aspects related to the problem of 3D effect and conclude the paper.

2. Methods and Data

2.1. Full-Waveform Inversion

In this study we consider velocity model building with acoustic isotropic FWI, which is a sufficient approximation to evaluate the out-of-plane wavefield propagation. Waveform modeling is performed with 2D and 3D

finite-difference time-domain modeling (2^{nd} order in time and 4^{th} order in space; TOYXDAC_TIME code (P. Yang et al., 2018). To minimize the computational costs we take advantage from the reciprocity of the Green's functions and we simulate the vertical force source at the OBS position and extract the pressure wavefield at the receivers placed at the air-gun shot position. Accurate positions of the sources and receivers in the finite difference grid is set using the sinc interpolation (Hicks, 2002). During modeling we allow for generation of the multiples from the free surface boundary imposed at the sea level.

For the inversion we use classical FWI formulation where the mismatch between observed $\mathbf{d}_{obs}$ and synthetic $\mathbf{d}_{cal}$ datasets generated with N_s sources and N_r receivers is expressed in the least squares sense as:

$$J(\mathbf{d}_{cal},\mathbf{d}_{obs}) = \frac{1}{2}\sum_{s=1}^{N_s}\sum_{r=1}^{N_r}\int_0^T (\mathbf{d}_{cal}(\mathbf{x}_r,t;\mathbf{x}_s) - \mathbf{d}_{obs}(\mathbf{x}_r,t;\mathbf{x}_s))^2 \mathrm{d}t, \tag{1}$$

where T is the recording time for the seismic trace associated with given source $\mathbf{x}_s$ and receiver $\mathbf{x}_r$. For a given model of physical parameters $\mathbf{m}$ the corresponding L^2 FWI misfit function can be written:

$$C(\mathbf{m}) = J(\mathbf{d}_{cal}[\mathbf{m}],\mathbf{d}_{obs}). \tag{2}$$

with $\mathbf{d}_{cal}[\mathbf{m}]$ corresponding to the synthetic data generated in this model.

During FWI the cost function C is minimized through local optimization techniques (Métivier & Brossier, 2016). Starting from an initial model $\mathbf{m}_0$, at each iteration k the updated model $\mathbf{m}_{k+1}$ is obtained as follows:

$$\mathbf{m}_{k+1} = \mathbf{m}_k + \Delta\mathbf{m}_k, \tag{3}$$

where $\Delta\mathbf{m}_k$ is the model update given by:

$$\Delta\mathbf{m}_k = -\alpha_k Q_k \nabla_{\mathbf{m}} C_k, \tag{4}$$

In Equation 4, $-\nabla_{\mathbf{m}}C$ is the steepest-descent direction, that is, the opposite direction of the gradient of the misfit function - where the gradient is computed with the adjoint-state method (Plessix, 2006). The gradient is scaled by α_k, a positive scalar estimated during the linesearch process (Nocedal & Wright, 2006) and Q_k is an approximation of the inverse Hessian computed following the l-BFGS strategy (Byrd et al., 1995), combined with a diagonal pseudo-Hessian approximation (Shin et al., 2001) acting as a preconditioner of the gradient and compensating for the amplitude decay with depth.

2.2. Data

Our numerical tests rely on the data generated in the GO_3D_OBS synthetic model of subduction zone (Górszczyk & Operto, 2021). The model was designed to test the performance of various regional-scale seismic imaging approaches dedicated to volumetric and geologically complex environments. From the full-scale model ($30 \times 175 \times 100$ km) we extract two 3D target Vp models of dimensions $30 \times 100 \times 20$ km presented in Figure 2. Both target models contain structurally complex part of the accretionary prism with highly deformed folds and major faults cutting through them. The strong velocity variations associated with these structures represent a challenge for velocity model reconstruction with seismic methods. The inline dimensions of the model from scenario I (Figure 2a) and II (Figure 2b) are roughly perpendicular and parallel to the axis of subduction front respectively. For both scenarios the OBS profiles are located along the central inline of the target model. Such experimental setting satisfy the geometry of the wide-angle OBS profiles acquired in subduction zones regions (see e.g. Figure 1 in Arnulf et al., 2022). From a structural point of view, the OBS profiles in scenario I and II cut along the dip and strike direction of subduction zone respectively. Accordingly, the changes in lithology and corresponding interfaces are expected to be roughly normal to the profile for scenario I and parallel for scenario II. In turn, from the point of view of wave propagation, for scenario I the wavefront shall maintain relative symmetry with respect to the axis of the profile, while for scenario II we expect channeling of the waves along the interfaces and structures with higher velocity that are not aligned with the profile. The data from scenario II shall, therefore, be significantly affected by 3D effect.

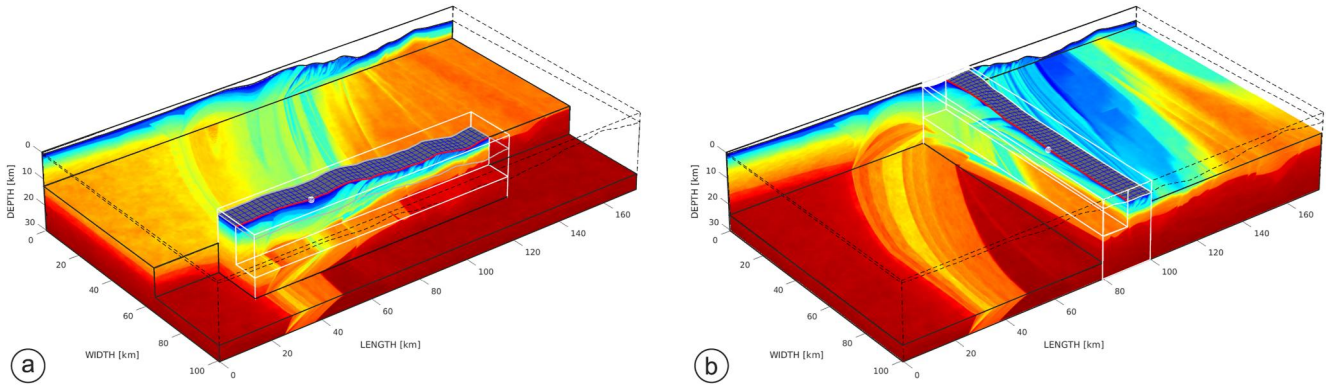

Figure 2. 3D target models extracted from the full GO_3D_OBS. Two models correspond to scenarios I (a) and II (b) with the inline direction of the models oriented roughly in the perpendicular (a) and parallel (b) manner to the subduction front. The red lines mark the central inlines of each target model and the white circles at the seabed mark the OBS positions for gathers presented in Figures 3 and 5.

To generate our testing datasets we design two 2D seismic profiles cutting through the center of the target models (see the red line in Figures 2a and 2b). Along these profiles, for each scenario, we generate two datasets assuming 2D and 3D wavefield propagation. In the first case we force the 2D wave propagation within the 2D models extracted along the central inlines that overlaps with the acquisition profile. 3D dataset is generated with the same acquisition parameters, but the wave propagation is now conducted within the 3D volume of the target models allowing waves to probe the area of the model that is not aligned with the 2D seismic profile. We simulate 40 OBS stations deployed with 2.4 km intervals and 999 shots with 100 m intervals. To mitigate the computational burden we use low-frequency data generated with 1.5 Hz Ricker source wavelet (max frequency ∼3.5 Hz) and propagate the wavefield for 21 s to reach the full-offset range (100 km). We assume acoustic wavefield propagation with constant density model.

3. Results

3.1. Experiment Setup

To test what is the influence of 3D effect on the 2D velocity model building we apply 2D FWI to the 2D and 3D datasets from scenario I and II. Initial FWI models are generated with a Gaussian smoothing applied to the true model. The smoothing parameters are tuned to remove most of the details from the true model without causing cycle-skipping. To focus only on the effect of out-of-plane propagation we invert the data without any band-pass filtering or added noise.

3.2. Scenario I

In Figures 3a and 3b we present OBS generated in the 2D and 3D models from scenario I (see Figure 2a for the OBS location). For seismograms in Figure 3b we applied 3D/2D phase correction (convolution in time with $\sqrt{t^{-1}}$) and amplitude correction (multiplication by $\sqrt{t}$ (Q. Yang et al., 2021). As expected, the simple amplitude scaling, which is routinely applied to correct from 3D to 2D amplitude decay, is not enough to match precisely the amplitudes of the data in Figure 3b to their 2D equivalent in Figure 3a (note difference in the colorscale in Figures 3a and 3b). In Figure 3c we present in the interleaved manner intervals of 50 seismograms from Figures 3a and 3b (shaded traces correspond to the data from the 2D model). One can observe that despite high complexity of the wavefield after the phase shift correction the continuity of the arrivals at the boundaries between subsequent intervals is preserved. This means the wavefield generated in the 3D model traveled the wavepath aligned with the axis of the profile. To visualize the wavepaths we compare the wavefield snapshots extracted from the modeling in 3D model and its 2.5D version (resulting form the projection of the central inline—2D model—toward crossline direction). In Figures 3d–3f and 3g–3i the 2.5D and 3D wavefield snapshots extracted at 6 s, 9, and 12 s are superimposed on the depth slices showing the velocity structure of the 2.5D and 3D models at 5 km depth. Indeed, the alignment of the geological structures in the 3D model that are nearly perpendicular to the profile (Figures 3g–3i) do not cause significant out-of-plane propagation and the corresponding wavefield snapshots are generally similar to those in Figures 3d–3f.

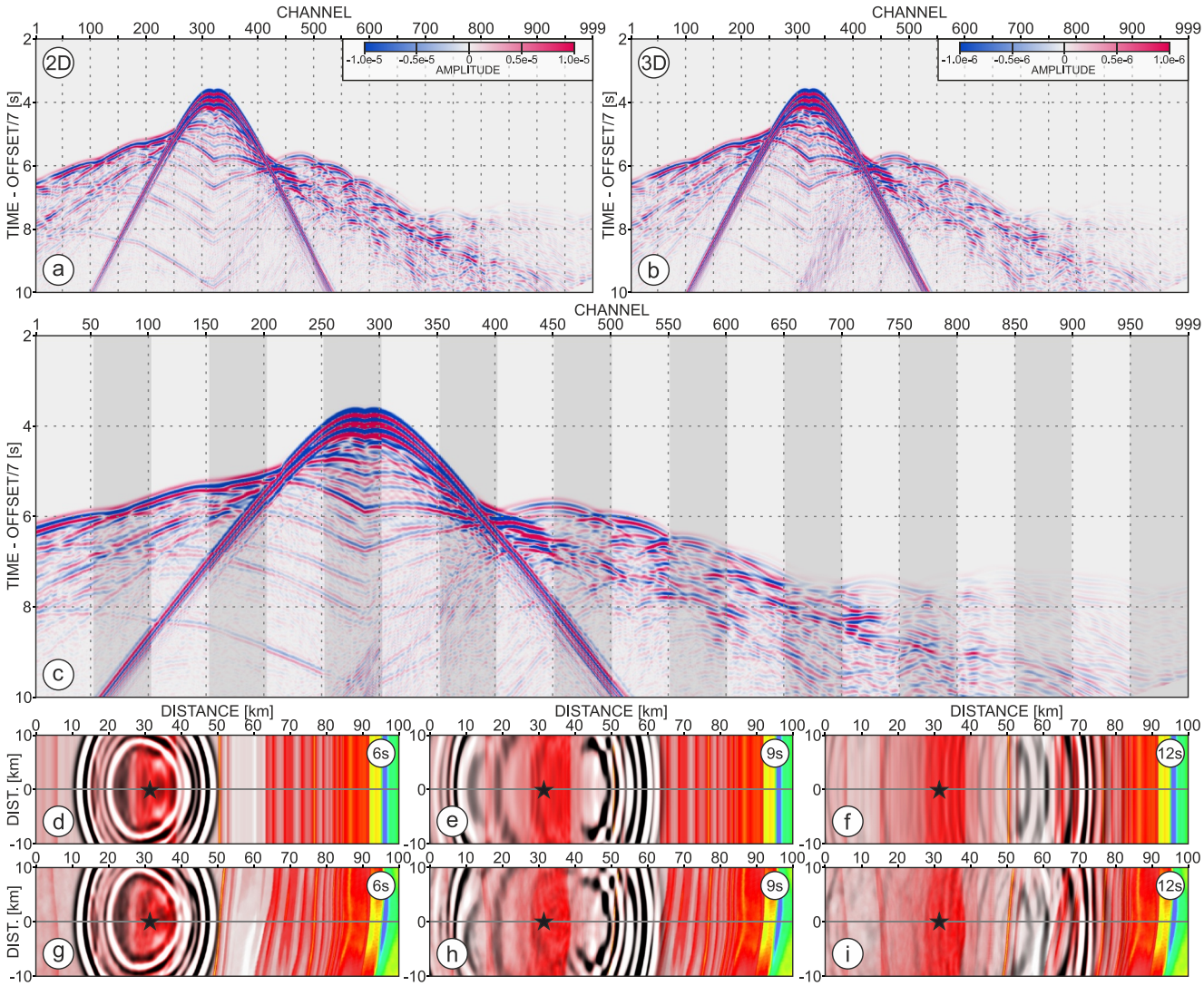

Figure 3. OBS gathers generated for scenario I in (a) 2D model, (b) 3D model. (c) OBS gather consisting of interleaved intervals of traces from (a) and (b). (d)–(f) and (g)–(i) Wavefield snapshots extracted after 6 s, 9 s, 12 s of propagation in scenario's I 2.5D and 3D model respectively.

In Figure 4a we show the true 2D inline *Vp* model extracted from the target model along the seismic profile. The initial model (Figure 4b) is generated with a Gaussian smoothing applied to the true model. In Figure 4c we show the perturbation model - namely the difference between the true and the initial model—that has to be recovered during FWI. During our acoustic FWI we invert for P-wave velocity (density model is homogeneous 1,000 kg/m^3) using 50 FWI iterations with L-BFGS optimization method.

Figure 4d shows the perturbations reconstructed by 2D FWI of 2D data. This FWI test can be considered a reference point inverse crime, since we use exactly the same experimental settings (modeling engine, acquisition geometry, source signature, density model, no noise) as for generating the input data, with the initial velocity model being the only difference. Not surprisingly, we were able to recover precisely velocity perturbations (compare Figures 4c and 4d), although the FWI resolution limited by the maximum inverted frequency (3.5 Hz) disallow for perfect reconstruction of the sharp interfaces (e.g., Moho). This is why, despite the fact that after 50 iterations the drop of the L^2 data misfit reaches 98%, the reduction of the model misfit is around 42% (see the inset in Figure 4d).

In the following test we apply 2D FWI to the 3D data. As we mentioned before, first we apply 3D/2D phase and amplitude corrections. However, since after amplitude correction (multiplication by $\sqrt{t}$) the seismograms

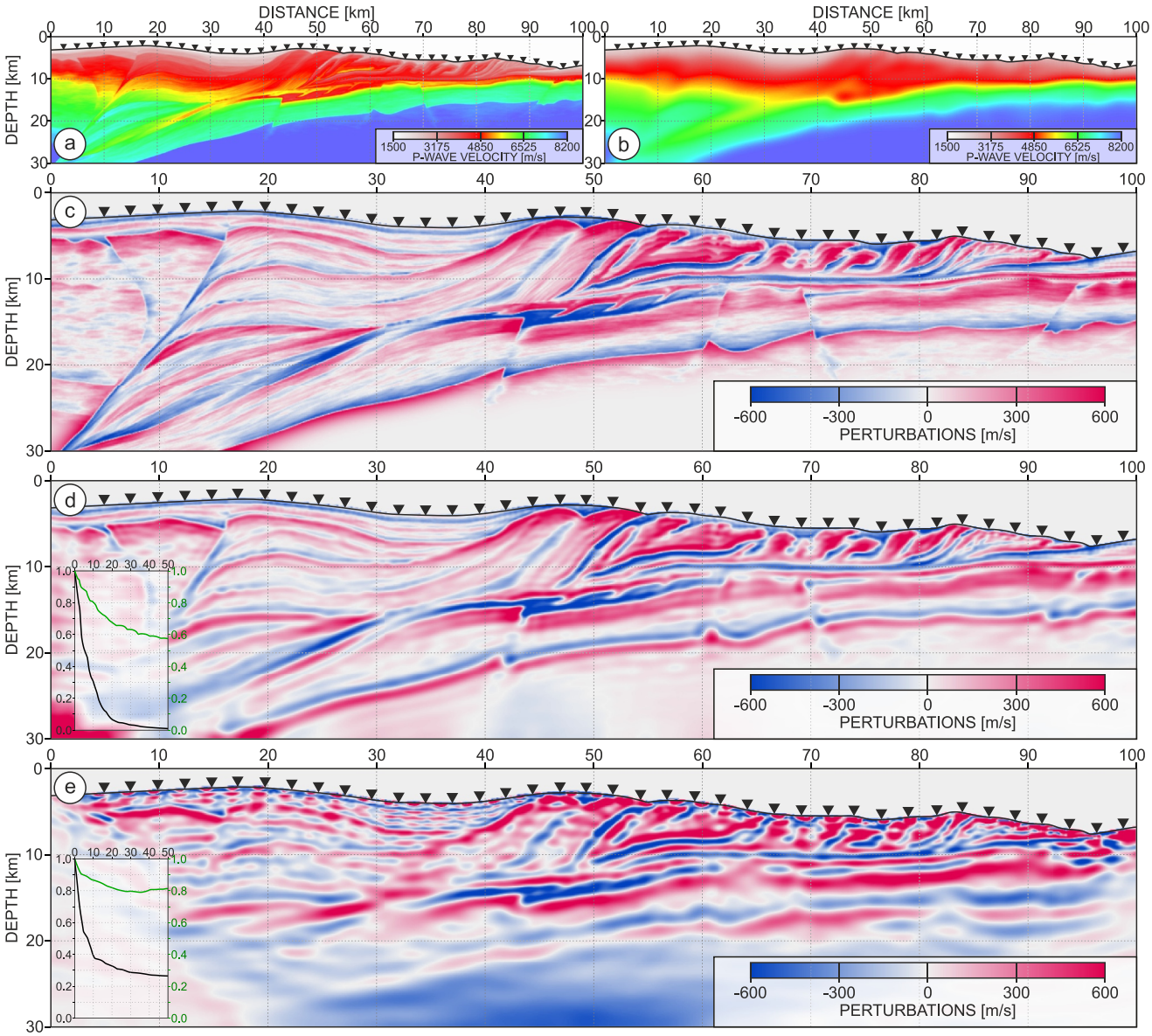

Figure 4. 2D true (a) and initial (b) velocity model for FWI in scenario (i) (c) Velocity perturbations—difference between (a) and (b). Final FWI perturbations from (d) 2D FWI of 2D data and (e) 2D FWI of 3D data. Insets in (d) and (e) show normalized L^2 data and model misfit reduction with FWI iterations (black and green line, respectively).

generated in 3D model does not match to the amplitudes of their 2D counterparts (see Figures 3a and 3b) we additionally scale the amplitudes of the source wavelet by the factor of 0.000375. We derive this value through a line search over different scaling factors, each time checking the misfit value at the initial FWI iteration and choosing the one that gives the smallest misfit (see Text S1 and Fig. S1 in Supporting Information S1). Despite this, the AVO trends in the corrected input OBS gathers and gathers modeled during FWI with the scaled source wavelet are still not the same. This fact is reflected by the perturbation model presented in Figure 4e, where the general shape of the velocity perturbations is reconstructed relatively well. However, due to the problem with the reconstruction of the AVO during our FWI, amplitudes of some parts of the data are underfitted - while others are already overfitted. This leads to the oversaturation of the velocity perturbations that causes accumulation of the kinematic error along the wavepath. General degradation of the reconstruction in the deeper parts of the model (where the wavefield illumination is reduced) is most likely caused to compensate for this kinematic error and maintain the phase matching. The overfitting of the data is also reflected by the plot in the inset of Figure 4e.

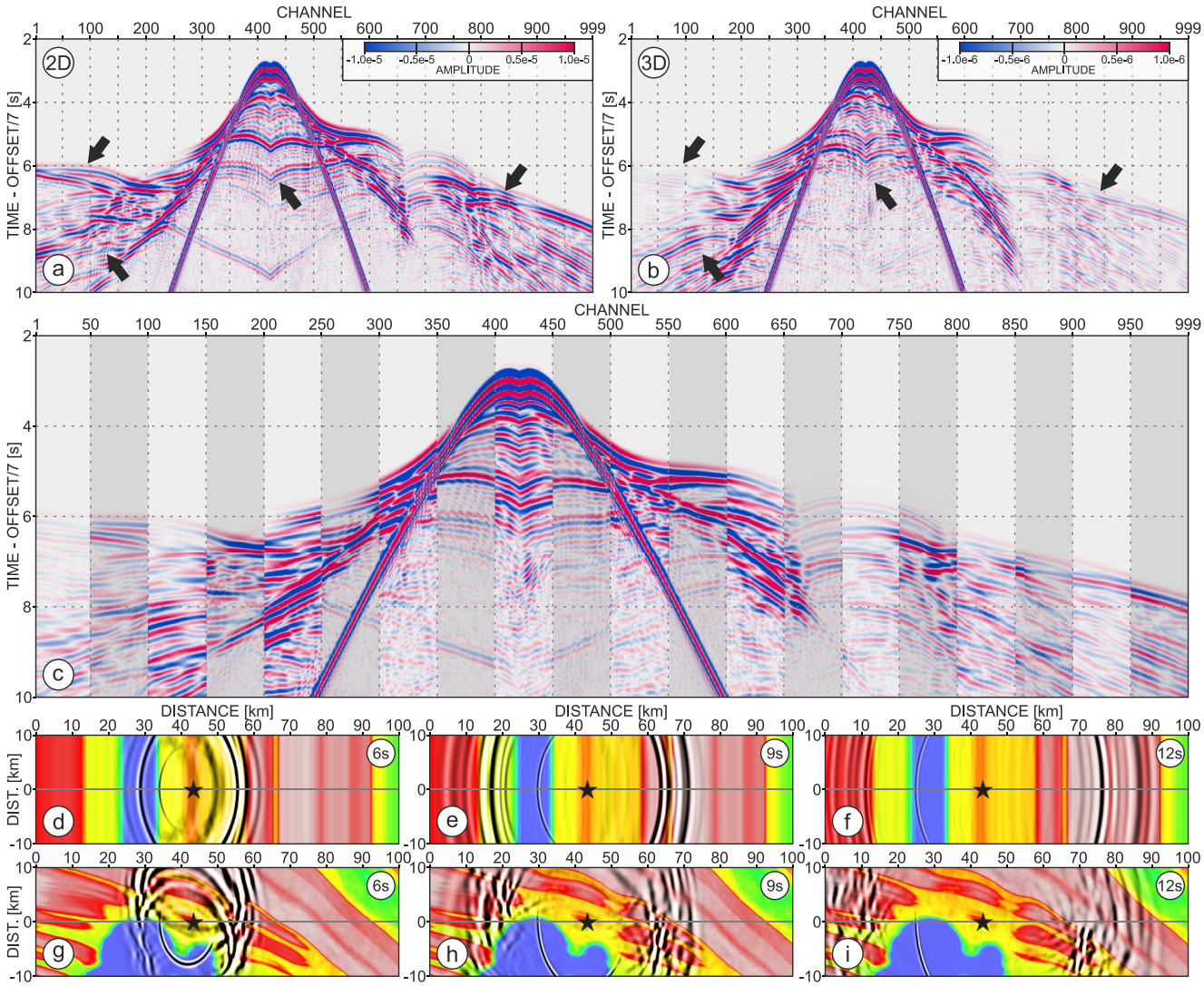

Figure 5. OBS gathers generated for scenario II in (a) 2D model, (b) 3D model. Black arrows indicate the most pronounced differences between two wavefields. (c) OBS gather consisting of interleaved intervals of traces from (a) and (b). (d)–(f) and (g)–(i) Wavefield snapshots extracted after 6 s, 9 s, 12 s of propagation in scenario's II 2.5D and 3D model, respectively.

While the black curve representing L^2 data misfit flattens after 50 iterations around 27%, the model misfit—denoted by green curve—drops only for 20% and starts to slowly increase after iteration 35.

The two tests presented here show that the 2D FWI has potential to recover meaningful structure from the data acquired in the 3D environment if they are not severely affected by the out-of-plane propagation. Here we consider classical FWI implementation with L^2 misfit function, which takes into account both phase and amplitude information and leads to the local over-and underfitting of the amplitudes. It is true that the velocity model reconstruction with FWI is mainly driven by the phase information, however, the amplitude mismatch can still introduce errors in the final model. The results in Figure 4e most likely leave room for further improvement with more elaborate multiscale FWI workflow—perhaps focusing more on amplitude normalization or phase only fitting.

3.3. Scenario II

In the same manner as for scenario I in Figures 5a and 5b we present the OBS gather generated for the OBS located in the central part of the 2D and 3D models from scenario II (see Figure 2b for the OBS location). The same amplitude and phase corrections as for scenario I are applied to the seismograms in Figure 5b. Unlike for

scenario I, the gathers in Figures 5a and 5b are significantly different. With black arrows we mark the most obvious differences not only in amplitudes but also in terms of position of various arrivals - first breaks as well as short-spread and wide-angle reflections. The differences are better underlined in the gather of interleaved 2D/3D seismograms in Figure 5c. Clearly, the mispositioned phases (except the water wave) at the edges between the groups of the seismograms indicate significant 3D effect for this scenario. Orientation of the acquisition profile in the parallel manner to the subduction front causes splitting and channeling of the wavefront along the geological structures characterized by different velocities as presented in Figures 5g–5i. The wavefield snapshots extracted during 3D modeling are very different from these generated in 2.5D model—Figures 5d–5f. In particular, one can observe how the wavefield lack symmetry with respect to the axis of the model and takes various wavepaths on the both side of the acquisition profile. This effect ultimately must cause problems for the 2D model reconstruction presented hereafter.

In Figures 6a and 6b we present the true and initial 2D model extracted along the central inline of the target model for scenario II (see Figure 2b). The difference between these models - namely the perturbation model—is presented in Figure 6c. Applying 2D FWI to the 2D data again leads to the good reconstruction of the velocity perturbations presented in Figure 6d. The normalized data misfit reduction is 99% and the respective model misfit drop is roughly 60% (we remind here the resolution limit of our FWI which hampers reconstruction of sharp interfaces). The 2D FWI of the 3D data for this scenario fails to converge to a meaningful reconstruction. In Figure 6e the reconstructed perturbations are meaningless indicating severe problems to find the 2D model that can explain the data with 3D effect. Interestingly, the inversion was able to run 50 iterations with significant drop of data misfit (around 80%) and at the same time, the model misfit increased by a factor of 4 with respect to the initial error. We have tried to improve the FWI performance by windowing the input data in time and offset domain, applying weighting with offset in the misfit function, re-estimating the source, changing the optimization scheme and gradient preconditioning, and so on. However, none of these approaches lead to substantial improvements—while some of them caused lack of convergence of FWI. For this case, we also analyze the performance of graph-space optimal transport misfit function (GSOT, Métivier et al. (2019)). The GSOT is the cost function with improved convexity which has potential to converge toward a correct solution despite cycle-skipping. Indeed, the perturbations in Figure 6f show some evidence of the original structure, however, the overall reconstruction of the model is still wrong, which is illustrated by the increasing model misfit (see the inset in Figure 6f). Therefore, we can conclude that the improved convexity of the cost function allows for a comparison of some shifted phases and introduce less artifacts related to the 3D effect than the classical L2-norm. However, it cannot compensate for the fact that these shifted arrivals are linked to the 3D-effect and cannot contribute to a meaningful geological reconstruction under the 2D approximation.

The two results presented in Figures 6e and 6f show how severely the results of 2D FWI from the 3D data can be affected by the 3D effect. In general the difficulties can be divided into fitting the amplitude information and phase information. The problem of amplitude mismatch between 2D and 3D data can be mitigated in different ways with more elaborate corrections and scaling or ultimately with misfit functions that do not consider AVO information—although at the cost of loss of information. The problem of 2D/3D mismatch of the phases, which is the driving factor of the kinematic accuracy of the reconstructed model, seems more severe. In the case where out-of-plane propagation leads only to the shifting of the arrivals in time the 2D inversion can still converge and explain the data. Even when local cycle-skipping occurs, more convex misfit functions have potential to fit the corresponding phases. Unfortunately, the model perturbations introduced during such 2D FWI will be biased by the inconsistency between the 3D wavepath and its projection on the 2D plane during 2D FWI. In more complex cases - as the one presented here in scenario II - out-of-plane propagation causes not only phase shifts but also generates the arrivals that are originating from the structures that are offset from the 2D profile and are not present in the 2D data. If these arrivals are used for 2D FWI, the inversion must fail as it will be unable to explain them by the geologically meaningful 2D structure. One possible way to evaluate how much the data are affected by the 3D effect is to perform a polarization analysis presented in the next section.

3.4. Polarisation Analysis

One of the advantages of the seismic surveys conducted with receivers deployed at the sea-floor—like the OBS surveys—is the ability to record 4-component seismic data. The richness of the recorded wavefields can be explored to better constrain mono-parameter P-wave velocity reconstruction or to reconstruct both P- and S-wave velocity models. Recent results of multi-parameter FWI in fluid-solid coupled medium (Cao et al., 2021) or

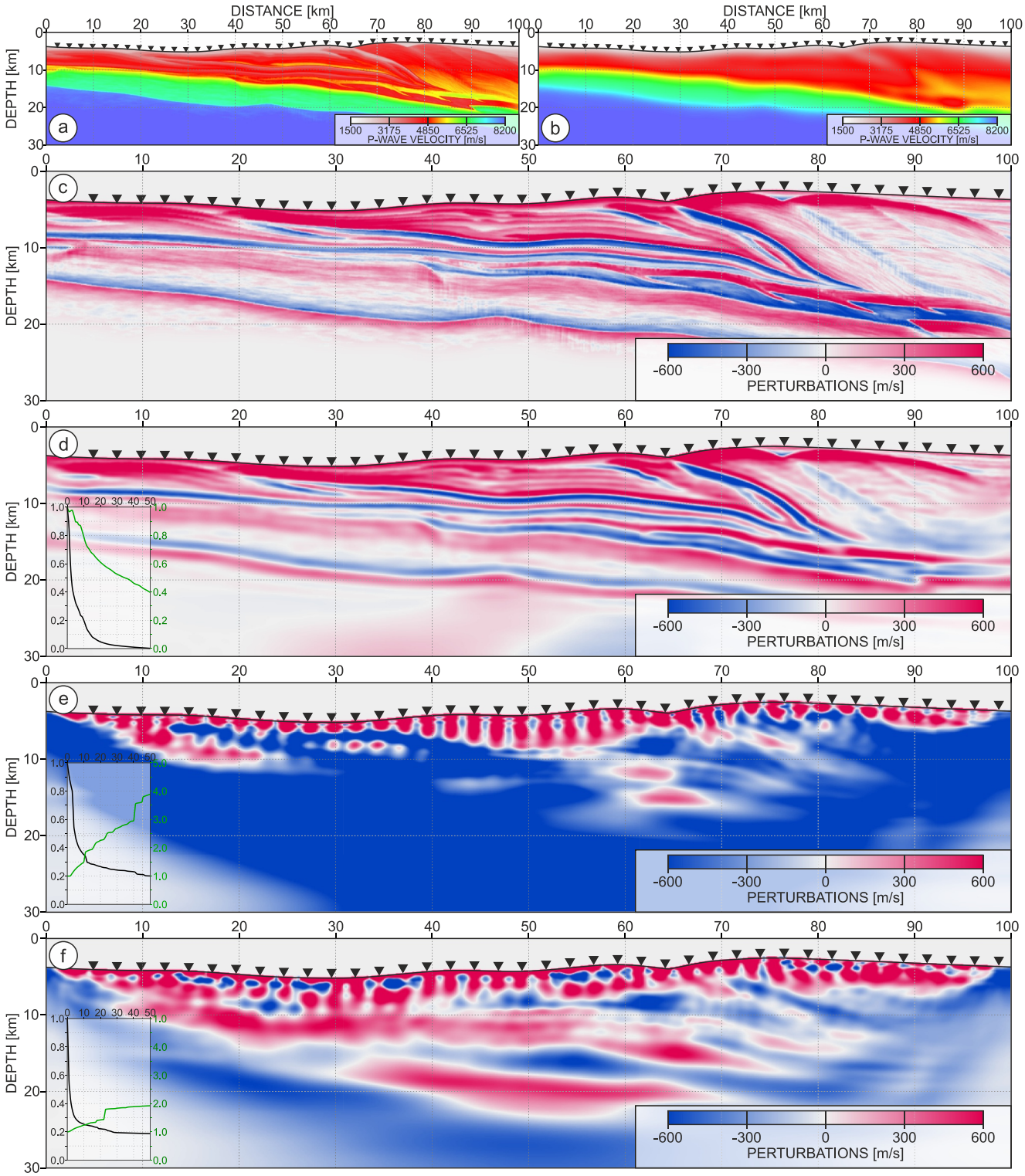

Figure 6. 2D true (a) and initial (b) velocity model for FWI in scenario II. (c) Velocity perturbations—difference between (a) and (b). Final FWI perturbations from (d) 2D FWI of 2D data; (e) 2D FWI of 3D data; (e) 2D GSOT-based FWI of 3D data. Insets in (d)–(f) show normalized L2 data and model misfit reduction with FWI iterations (black and green line respectively).

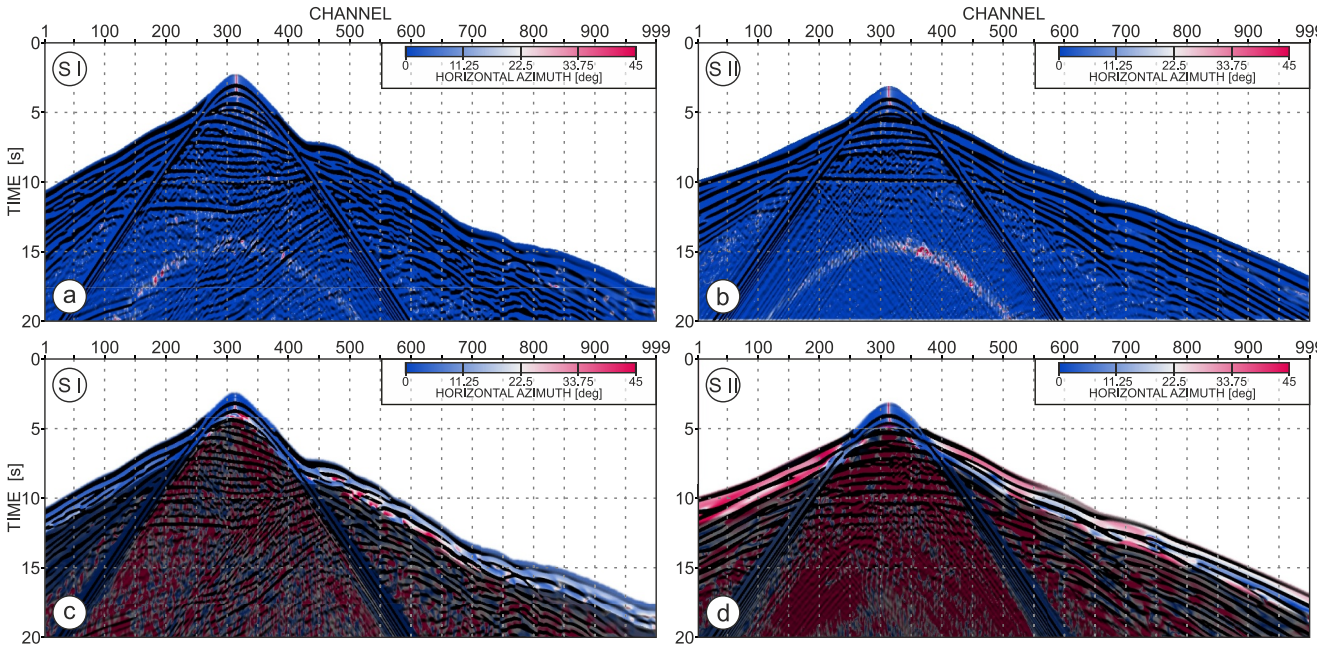

Figure 7. Examples of 2D OBS gathers for scenario (a) I and (b) II superimposed on the on the colormap representing horizontal azimuth angle of the wavefield at the receiver location. Panels (c) and (d) show the same analysis for corresponding 3D OBS gathers. Shaded areas in (c) and (d) cover the part of the wavefield where the polarization analysis is biased by interfering arrivals.

polarization-based FWI misfit function (Sambolian et al., 2022) demonstrated great potential of multicomponent seismic data for reconstruction of subsurface models in marine environment. In this study we perform polarization analysis (available in Seismic Unix toolbox; Cohen & Stockwell, 2008) to estimate the horizontal azimuth angle of the wavefield (see φ in Figure 1b) at the airgun shot position - namely receiver position within the reciprocity rule considered in this study. In the idealized assumption of 2D seismic experiment (namely without 3D effect) the wavepath follows the plane of the profile and therefore the horizontal azimuth angle shall be 0. This situation is illustrated in Figures 7a and 7b, where two gathers generated in 2.5D versions of models from scenario I and II respectively are superimposed on the value of the horizontal azimuth angle at the receiver location. In 2.5D medium there is no lateral velocity variation along the strike direction, and therefore there is no out-of-plane wavefield propagation (see the symmetric wavefront in Figures 3d–3f and Figures 5d and 5f). Indeed, in Figures 7a and 7b the calculated horizontal azimuth is nearly everywhere equal to 0 - blue color (hyperbolic bands of light-red color at the later times are most likely due to the imperfect absorbing boundary condition at the bottom-edge of the model). The situation changes drastically when instead of 2.5D models we consider the true 3D models for both scenarios. In case of scenario I (Figure 7c) we can still observe that the horizontal azimuth of early arrivals is close to 0 (blue and light blue color). However, for the gather from scenario II (Figure 7d) we observe that the horizontal azimuth of early arrivals can reach more than 40° (e.g., red color between channels 1 and 250) and can vary along the offset depending on the type of arrival (see variations between blue and red color starting from channel 400 to 999). This analysis, though efficient when considering only pure wave modes (in our case early P-wave arrivals), demonstrates how polarization analysis can be helpful in evaluating the 3D effect in the seismic data acquired along the 2D profiles.

3.5. 3D FWI

Intuitive panacea solving the problem of the out-of-plane wavefield propagation is to account for it at the velocity model building stage. When FWI is considered this can be achieved through an application of 3D rather 2D waveform modeling and inversion of the seismic data acquired along the 2D profiles. Extensions of the model space toward third dimension shall allow for free wavefield propagation along all directions, and therefore provide closer representation of the field experiment. To test this hypothesis here we consider the dataset from scenario II, where the 2D FWI of the data generated in the 3D model was unable to converge toward meaningful reconstruction (Figure 6e). Instead of using 2D FWI we now process exactly the same dataset but applying 3D

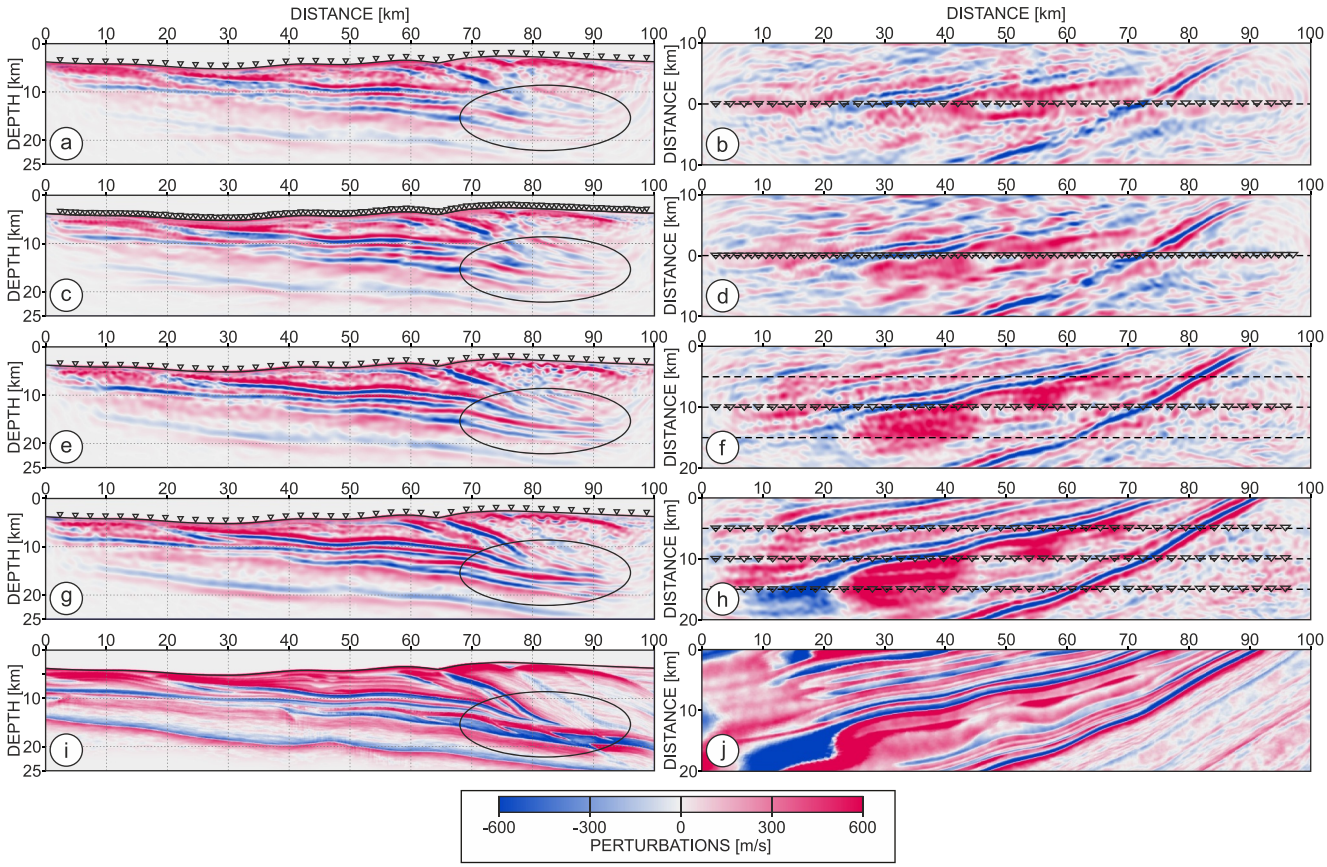

Figure 8. Velocity perturbations recovered with 3D FWI for scenario II using (a)–(b) 40 OBS, 1 receiver line and 1 shooting line; (c)–(d) 120 OBS; 1 receiver line and 1 shooting line; (e)–(f) 40 OBS; 1 receiver line and 3 shooting lines; (g)–(h) 120 OBS; 3 receiver lines and 3 shooting lines. (i)–(j) True perturbations. Left and right panels show perturbations extracted along central inline and depth-slice at 8 km of model depth, respectively. Triangles mark the OBS positions and dashed lines mark the shooting profiles. Black ellipse in left panels mark the complex target that is the most problematic to recover.

FWI starting from the smooth 3D initial model. Figures 8a and 8b present the reconstructed velocity perturbations (after 120 FWI iterations) along the central inline coinciding with the 2D acquisition profile and the depth slice extracted at 8 km of model depth respectively. Unlike in case of 2D FWI (Figure 6e), this time the inversion converges toward correct model—though its deeper part is not well reconstructed (compare with true perturbations in Figure 8i). Specifically, there is a problem with correct imaging of complex structure around 80 km of model distance below 10 km of depth marked by black ellipse in Figure 8. On the depth-slice in Figure 8b one can observe that the reconstruction is focused mainly around the acquisition profile and become noisy with the increasing distance from its axis—which is intuitive.

Despite imperfect model reconstruction (comparing to model in Figure 6d) the 3D FWI was able to handle the out-of-plane wavefield propagation and produce geologically consistent models. Mentioned errors in the final model come from the faster accumulation of kinematic error in case of 3D FWI rather than its 2D version due to the additional degree of freedom of wave propagation associated with horizontal azimuth angle φ (Figure 1b). We can now consider different scenarios to solve this problem at the acquisition design stage. In the following test we assume denser 2D deployment of 120 receivers instead of previously considered 40. The results after 120 FWI iterations are presented in Figures 8c and 8d. Though one can observe an increased continuity of the recovered interfaces the problem of recovering the deep complex structures remains. The depth-slice in Figure 8d appears less noisy but the velocity structure away from the 2D acquisition profile is still blurry. The third acquisition we consider here consist of a 2D deployment of 40 OBS stations and 3 shooting lines—one over the OBS profile and two ±5 km from the OBS profile in crossline direction (see Figure 8f). With 40 OBS the reconstruction becomes noisier (comparing to 120 OBS) but importantly, the region marked by black ellipse in Figure 8e is now better reconstructed. Comparing the depth-slices in Figures 8b and 8f, we can clearly observe how with the same number

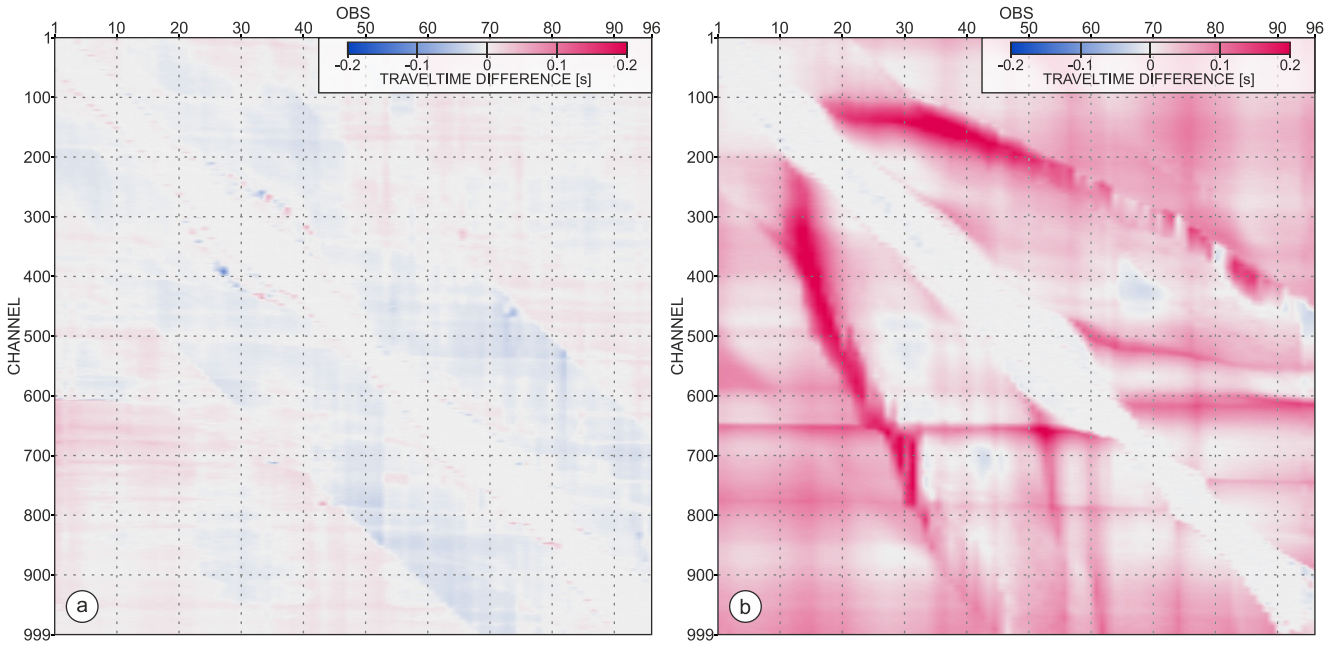

Figure 9. Difference between the first-arrival traveltimes generated in 3D and 2.5D models from (a) scenario I and (b) scenario II.

of 40 OBS but additional shooting lines we improve the reconstruction of the velocity model away from the OBS profile. The obtained model is also better reconstructed than in case of 2D acquisition with 120 OBS (compare Figures 8d and 8f). Finally we consider a deployment of three OBS and three shooting profiles (40 OBS each; see Figure 8h). The resulting model clearly demonstrates the superior reconstruction among all considered acquisition geometries. Despite narrow azimuth coverage, we recover 3D extension of the structure along the crossline direction of the model (Figure 8h). Also the problematic structure marked by black ellipse in Figure 8g is better recovered. Importantly, the final model in Figure 8g is better reconstructed comparing not only to model in Figure 8a but also Figure 8c. This means that in complex media oversampled 2D OBS deployment may still lead to lower quality imaging than a sparser 3D OBS deployment of the same number of receivers.

4. Discussion

4.1. 3D Effect in FAT

2D waveform inversion methods like FWI seem prone to errors associated with 3D effect due to their limited tolerance to the discrepancy in the input data. In other words, if during the 2D FWI the out-of-plane waveforms are fitted, then it must lead to a wrong velocity model reconstruction. On the other hand, if such waveforms are not fitted during 2D FWI or are not reconstructed in the synthetic data, then the mismatch leaks into the associated adjoint source and is consequently accommodated into velocity model update—though toward wrong direction. However, the 3D effect shall not only influence the velocity model building with 2D FWI but also traveltime tomography—even when we consider only first-arrival traveltimes as in case of FAT. In Figure 9 we show the first-arrival traveltimes differences between the traveltimes picked from 2D and 3D data organized in OBS versus channel coordinates. The traveltimes were picked using STA/LTA algorithm and manually corrected for the outliers. One can observe that the traveltime differences for scenario I (Figure 9a) can be considered negligible, however they are significantly higher for scenario II(Figure 9b). Generally, the red color in the traveltime map means that the 3D traveltimes are faster than their 2D counterpart. Locally the difference between two traveltimes reaches more than 0.45 s. We do not consider detailed analysis of 2D FAT approach and results here, however, it is clear that this range of traveltime error caused by 3D effect has impact on the reconstruction of smooth FAT model and can potentially lead to misinterpretation of large-scale structures. Resulting 2D FAT velocity models and their description are presented in supporting information (Fig. S2 and Text S2 in Supporting Information S1). It is also worth to consider what is the meaning of routinely used total root mean square (RMS) traveltime error in

such case. Indeed, forcing the 2D FAT to fit the out-of-plane traveltimes will lead to decreasing of RMS error, but at the same time it will increase the actual error in velocity model reconstruction.

4.2. Acquisition Logistics

In the 3D FWI examples presented in Figure 8 we have considered few ad hoc acquisition approaches. Moving from a single 2D seismic profile to the 3D experiment consisting of three such 2D profiles obviously generates additional financial burden. On the other hand, the benefit of having an access to the 3D extension of the geological structure (compare Figures 8b and 8h) is also clear and priceless from the point of view of geological interpretation. The fundamental factor for choosing between 2D and 3D OBS acquisition is therefore the expected complexity of the investigated target. While for the environments with lack or little velocity variations along the crossline direction the 2D acquisition is probably enough, then for more heterogeneous media the 3D acquisition geometry shall be considered. Here we considered 120 OBS stations, which in the similar range as 100 OBS used during SFJ-OBS survey in 2001 (Górszczyk et al., 2017). Therefore gathering the similar pool of OBS nowadays (and their deployment) shall not be a prohibitive factor for 3D academic surveys. A more challenging aspect is related to increased time of shooting operation. Registration of far-offset seismic data (∼100 km) requires long listening time and therefore sufficient breaks (low speed of the seismic vessel) between consecutive airgun shots to avoid interference with water-wave of previous shot. Alternatively, the shots could be fired in two passes of the vessel (forward and back the line) in the interleaved mode at each second shot position but this effectively increases the sailed distance twice. To mitigate this issue, more advanced shooting approaches based on the source blending/deblending (Berkhout et al., 2008) could be considered. The efficient shooting approach shall be further coupled with optimized source/receiver spacing providing good illumination of the geological target (e.g., Abdellaziz et al., 2023; Guo et al., 2023; Krampe et al., 2020; Maurer et al., 2017; Vermeer, 2003; Wu et al., 2022) and supported at the processing stage by regularization approaches that are robust against sparse seismic acquisition (e.g., Aghamiry et al., 2021; D. Li & Harris, 2018; Zand et al., 2024; Zhu et al., 2017). Successful tuning of all these parameters can only be possible if the seismic experiment is prepared for the purpose of reconstruction of certain target using specific imaging technique. Synthetic modeling shall therefore be one of the key points to consider allowing optimization of the large scale 3D OBS surveys.

4.3. Computational Costs of 3D FWI

Moving from 2D to 3D FWI velocity model building brings additional burden in terms of availability of high performance computing (HPC) resources and robust source-code implementations. Though it might indeed be a barrier the additional expense comparing to the cost of seismic survey itself is rather minor. The computing power available under CPU or GPU architecture in HPC centers or cloud computing services is still increasing and shall be efficiently utilized by well optimized modeling and inversion codes. In our acoustic time-domain 3D FWI we consider relatively low frequency band of seismic data (up to 3.5 Hz). 3D model dimension was $25 \times 100 \times 20$ km (100 m grid space). We used 21 s of wavefield propagation, which allowed to accommodate full offset-range of the generated data. During computation we used two levels of parallelism offered by TOYXDAC_TIME code with one MPI process and six OpenMPI threads per OBS—leading to total number of 720 cores (120 OBS × 6 OpenMPI threads; 30 nodes × 24 cores). In such configuration it took c.a 1 hr per single FWI iteration. Inversion of higher frequencies would ultimately require resampling of the computing grid automatically increasing the demand of computing resources. Computing complexity of time-domain FWI scales with number of time-steps to $\mathcal{O}(N)$, number of sources to $\mathcal{O}(N^2)$ and dimension to $\mathcal{O}(N^2)$ in 2D and to $\mathcal{O}(N^3)$ in 3D. Therefore, if the frequency range of the data is doubled the computational time of 3D time-domain FWI will increase by factor of 16. This can be mitigated by another level of MPI parallelism over the decomposed model domain, which allows to involve more cores and reduce the computing time. Alternatively, frequency-domain FWI (theoretical computing complexity $\mathcal{O}(N^6)$) can also be considered for stationary receiver seismic acquisition like the one considered in this study. Though limited by memory requirement, this approach has its advantage in terms of fast wavefield recomputation for large number of seismic sources once the LU factorization of so called impedance matrix is performed. Recently Operto et al. (2023) demonstrated feasibility of this approach solving forward problem with the massively-parallel multifrontal direct solver MUMPS, when applying FWI to the moderate scale 3D real-data from the Gorgon field (650 OBS). Generally each FWI approach has its pros and cons and can be more favorable for specific application in terms of computational burden (depending on approximation of physics, size of computing domain, number of sources, acquisition geometry, frequency band, etc.). In any case, HPC resources

available by computing centers make it possible to apply 3D (acoustic) FWI in regional scale (Morgan et al., 2013) routinely rather than exceptionally - which is confirmed by the fact the it is now standard in oil & gas exploration industry.

4.4. 3D FWI of 2D OBS Data

In Section *3D FWI* we presented the FWI approach where data from 2D OBS profile affected by 3D effect are processed within the 3D models, which allowed the inversion to converge toward the correct direction of reconstruction (Figures 8a–8d). 3D FWI—on top of natural ability to handle the 3D effect—is also more consistent with the field data in the sense that it can account for the true position of the shot/receiver (e.g., when due to the currents the OBS is pushed offset from the 2D profile—especially at deep water). Moreover, during 3D FWI the input data do not require amplitude trend and phase adjustments from 3D to 2D geometrical spreading—that typically provide only crude corrections. One obstacle for practical application of the proposed approach might be the building of the initial FWI model (typically derived with ray-based FAT), which would already incorporate the velocity variations along the crossline direction. In our synthetic test we used the smooth version of the true model eliminating this problem. However, in case of real 2D OBS data, recovering velocity perturbations that offset from the seismic profile might not be straightforward if there is no additional shot or receiver coverage on both side of the 3D profile. Information that might be possibly used to force the 3D propagation during FAT initial model building is the horizontal azimuth angle—as it is estimated in Figure 7d. Using this information to shoot the ray with a given azimuth would force the propagation on the side of the profile axis and could potentially lead to correct initial model—in the sense that the smooth velocity variations along crossline direction are properly reconstructed. Another possibility to extract information about the underlying 3D structure is to analyze regional seismicity data in the area of the OBS profile. While this approach is theoretically sound and potentially valuable, there are practical challenges associated with data availability, spatial coverage, and the resolution limits of the models resulting from this type of analysis. Ideally, therefore, this issue shall be addressed at the acquisition design step with either additional shooting lines (Figure 8f) either narrow-azimuth 3D OBS survey incorporating certain number of OBS and shooting profiles.

5. Conclusions

Reconstruction of physically and structurally complex subsurface geological settings will always require certain level of approximation in terms of parametrization and spatial probing of the target. While the development of robust seismic imaging and inversion techniques obtained over last decade is striking, its application for crustal-scale academic seismic studies is often prohibitive due to the deficiency of the high-quality data. In particular, the paradigm of acquiring 2D OBS profiles in geologically complex environments causing 3D-effect may be no longer valid if one aims at high-resolution model reconstruction. We show how the data from the 2D acquisition can be biased by out-of-plane wavefield propagation and how this effect influences further velocity model building with FWI. Comparison of various ad hoc 2D and 3D OBS survey configurations coupled with 3D FWI clearly demonstrates how the model reconstruction and its geological interpretation can benefit from 3D OBS experiments. In a broader perspective, overcoming the limitations tied to 2D velocity model reconstruction opens up opportunities for advancing the exploration of FWI in multi-parameter model reconstruction. Achieving a more realistic parameterization of the subsurface, including elastic, viscoelastic, and anisotropic properties, necessitates high-quality datasets to minimize cross-talk between parameters and mitigate the leakage of acquisition-related artifacts into specific model. Complex geological settings, such as subduction zones, offer an ideal environment for conducting multi-parameter studies. However, their effectiveness relies on the seismic surveys being pre-designed to specifically accommodate this type of investigation. It is worth to mention that in this study we consider classical FWI approach without any sophisticated sparsity-promoting regularization, compressive sensing methods or optimized acquisition design. Integrating this kind of solutions to FWI workflow can further help to reduce the logistic overburden associated with moving from 2D to 3D OBS deployment and shooting, and optimize the acquisition parameters for future academic regional-scale seismic surveys.

Data Availability Statement

The GO_3D_OBS synthetic model (Górszczyk & Operto, 2021) can be accessed through the official data portal of IG PAS (https://dataportal.igf.edu.pl/dataset/go_3d_obs). The modeling and inversion code

TOYXDAC_TIME is developed within the framework of SEISCOPE project, sponsored by the private companies, which makes it unavailable for open access.

Acknowledgments
This study was partially funded by: (a) the Polish National Science Center (Grant 2019/33/B/ST10/01014); (b) the SEISCOPE project (http://seiscope2.osug.fr), sponsored by AKERBP, CGG, CHEVRON, EQUINOR, EXXON-MOBIL, JGI, PETROBRAS, SCHLUMBERGER, SHELL, SINOPEC, SISPROBE, and TOTAL). We thank Wojciech Gajek for picking the first breaks presented in Figure 9, Serge Sambolian for fruitful discussion about the polarisation analysis and Stéphane Operto for his valuable comments and the internal review of the paper. We extend our appreciation to the reviewers and editors for their constructive feedback, which contributed to refinement of this article. In this study we use TOYXDAC_TIME time-domain FWI code developed within the SEISCOPE project. The study was granted access to the HPC PL-Grid Infrastructure (grant id: plg3dwind4).

References

Abdellaziz, M., Brossier, R., Métivier, L., & Oudet, É. (2023). Optimal experimental design in full waveform inversion. In *84th EAGE annual conference and exhibition*. European Association of Geoscientists & Engineers. https://doi.org/10.3997/2214-4609.202310605

Abramovitz, T., Berthelsen, A., & Thybo, H. (1997). Proterozoic sutures and terranes in the southeastern Baltic Shield interpreted from BABEL deep seismic data. *Tectonophysics*, *270*(3–4), 259–277. https://doi.org/10.1016/s0040-1951(96)00213-2

Adamczyk, A., Malinowski, M., & Górszczyk, A. (2015). Full-waveform inversion of conventional vibroseis data recorded along a regional profile from southeast Poland. *Geophysical Journal International*, *203*(1), 351–365. https://doi.org/10.1093/gji/ggv305

Aghamiry, H., Gholami, A., & Operto, S. (2021). *On the robustness of sparsity-promoting regularized wavefield inversion with phase retrieval against sparse long-offset acquisitions, 82nd CAGE Annual Conference and Exhibition*. European Association of Geoscientists & Engineers. https://doi.org/10.3997/2214-4609.202011479

Arnulf, A. F., Bassett, D., Harding, A. J., Kodaira, S., Nakanishi, A., & Moore, G. (2022). Upper-plate controls on subduction zone geometry, hydration and earthquake behaviour. *Nature Geoscience*, *15*(2), 143–148. https://doi.org/10.1038/s41561-021-00879-x

Beller, S., Monteiller, V., Combe, L., Operto, S., & Nolet, G. (2018). On the sensitivity of teleseismic full waveform inversion to earth parametrisation, initial model and acquisition design. *Geophysical Journal International*, *212*(2), 1344–1368. https://doi.org/10.1093/gji/ggx480

Berkhout, A. J. G., Blacquière, G., & Verschuur, E. (2008). From simultaneous shooting to blended acquisition. In *SEG technical program expanded abstracts 2008*. Society of Exploration Geophysicists. https://doi.org/10.1190/1.3063933

Beylkin, G. (1987). Mathematical theory for seismic migration and spatial resolution. In M. Bernabini, P. Carrion, G. Jacovitti, F. Rocca, S. Treitel, & M. Worthington (Eds.), *Deconvolution and inversion* (pp. 291–304). Blackwell scientific publications.

Boddupalli, B., Minshull, T. A., Morgan, J., Bayrakci, G., & Klaeschen, D. (2021). Comparison of 2-D and 3-D full waveform inversion imaging using wide-angle seismic data from the Deep Galicia Margin. *Geophysical Journal International*, *227*(1), 228–256. https://doi.org/10.1093/gji/ggab164

Byrd, R. H., Lu, P., Nocedal, J., & Zhu, C. (1995). A limited memory algorithm for bound constrained optimization. *SIAM Journal on Scientific and Statistical Computing*, *16*(5), 1190–1208. https://doi.org/10.1137/0916069

Cao, J., Brossier, R., Górszczyk, A., Métivier, L., & Virieux, J. (2021). 3-D multiparameter full-waveform inversion for ocean-bottom seismic data using an efficient fluid–solid coupled spectral-element solver. *Geophysical Journal International*, *229*(1), 671–703. https://doi.org/10.1093/gji/ggab484

Carbonell, R., Gallart, J., Pérez-Estaún, A., Diaz, J., Kashubin, S., Mechie, J., et al. (2000). Seismic wide-angle constraints on the crust of the southern Urals. *Journal of Geophysical Research*, *105*(B6), 13755–13777. https://doi.org/10.1029/2000jb900048

Christeson, G. L., Avendonk, H. J. A. V., Norton, I. O., Snedden, J. W., Eddy, D. R., Karner, G. D., & Johnson, C. A. (2014). Deep crustal structure in the eastern Gulf of Mexico. *Journal of Geophysical Research: Solid Earth*, *119*(9), 6782–6801. https://doi.org/10.1002/2014jb011045

Cohen, J. K., & Stockwell, J. J. W. (2008). *CWP/SU: Seismic Unix release No. 41: An open source software package for seismic research and processing*. Center for Wave Phenomena, Colorado School of Mines.

Collins, J. A., Purdy, M. G., & Brocher, T. M. (1989). Seismic velocity structure at deep sea drilling project site 504B, Panama Basin: Evidence for thin oceanic crust. *Journal of Geophysical Research*, *94*(B7), 9283–9302. https://doi.org/10.1029/jb094ib07p09283

Corbalán, A., Nedimović, M. R., Louden, K. E., Cannat, M., Grevemeyer, I., Watremez, L., & Leroy, S. (2021). Seismic velocity structure along and across the ultraslow-spreading southwest Indian ridge at 64°30'E showcases flipping detachment faults. *Journal of Geophysical Research: Solid Earth*, *126*(10). https://doi.org/10.1029/2021jb022177

Fujie, G., Kodaira, S., Sato, T., & Takahashi, T. (2016). Along-trench variations in the seismic structure of the incoming Pacific plate at the outer rise of the northern Japan Trench. *Geophysical Research Letters*, *43*(2), 666–673. https://doi.org/10.1002/2015gl067363

Funck, T., Louden, K. E., & Hall, J. (2001). Wide-angle reflectivity across the Torngat Orogen, NE Canada. *Geophysical Research Letters*, *28*(18), 3541–3544. https://doi.org/10.1029/2001gl012959

Gorszczyk, A., Operto, S., Schenini, L., & Yamada, Y. (2019). Crustal-scale depth imaging via joint FWI of OBS data and PSDM of MCS data: A case study from the eastern nankai trough. *Solid Earth*, *10*(3), 765–784. https://doi.org/10.5194/se-10-765-2019

Grevemeyer, I., Ranero, C. R., Papenberg, C., Sallares, V., Bartolomé, R., Prada, M., et al. (2022). The continent-to-ocean transition in the Iberia Abyssal plain. *Geology*, *50*(5), 615–619. https://doi.org/10.1130/g49753.1

Guo, Y., Lin, R., & Sacchi, M. D. (2023). Optimal seismic sensor placement based on reinforcement learning approach: An example of OBN acquisition design. *IEEE Transactions on Geoscience and Remote Sensing*, *61*, 1–12. https://doi.org/10.1109/tgrs.2023.3247593

Gómez de la Peña, L., Grevemeyer, I., Kopp, H., Díaz, J., Gallart, J., Booth-Rea, G., et al. (2020). The lithospheric structure of the Gibraltar arc system from wide-angle seismic data. *Journal of Geophysical Research: Solid Earth*, *125*(9). https://doi.org/10.1029/2020jb019854

Górszczyk, A., & Operto, S. (2021). GO_3D_OBS: The multi-parameter benchmark geomodel for seismic imaging method assessment and next-generation 3D survey design (version 1.0). *Geoscientific Model Development*, *14*(3), 1773–1799. https://doi.org/10.5194/gmd-14-1773-2021

Górszczyk, A., Brossier, R., & Métivier, L. (2021). Graph-space optimal transport concept for time-domain full-waveform inversion of ocean-bottom seismometer data: Nankai trough velocity structure reconstructed from a 1D model. *Journal of Geophysical Research: Solid Earth*, *126*(5), e2020JB021504. https://doi.org/10.1029/2020JB021504

Górszczyk, A., Operto, S., & Malinowski, M. (2017). Toward a robust workflow for deep crustal imaging by FWI of OBS data: The eastern nankai trough revisited. *Journal of Geophysical Research: Solid Earth*, *122*(6), 4601–4630. https://doi.org/10.1002/2016jb013891

Heath, B. A., Hooft, E. E. E., Toomey, D. R., Papazachos, C. B., Nomikou, P., Paulatto, M., et al. (2019). Tectonism and its relation to magmatism around santorini volcano from upper crustal p wave velocity. *Journal of Geophysical Research: Solid Earth*, *124*(10), 10610–10629. https://doi.org/10.1029/2019jb017699

Hicks, G. J. (2002). Arbitrary source and receiver positioning in finite-difference schemes using Kaiser windowed sinc functions. *Geophysics*, *67*(1), 156–165. https://doi.org/10.1190/1.1451454

Jack, I. (2021). *Ocean bottom marine seismic methods*. In *Integration of geophysical technologies in the petroleum industry* (pp. 220–271). Cambridge University Press. https://doi.org/10.1017/9781108913256.007

Janik, T., Wójcik, D., Ponikowska, M., Mazur, S., Skrzynik, T., Malinowski, M., & Hübscher, C. (2022). Crustal structure across the Teisseyre-Tornquist Zone offshore Poland based on a new refraction/wide-angle reflection profile and potential field modelling. *Tectonophysics*, *828*, 229271. https://doi.org/10.1016/j.tecto.2022.229271

Kalinicheva, T., Warner, M., & Mancini, F. (2020). Full-bandwidth FWI. In *SEG technical program expanded abstracts 2020*. Society of Exploration Geophysicists. https://doi.org/10.1190/segam2020-3425522.1

Kamei, R., Pratt, R. G., & Tsuji, T. (2013). On acoustic waveform tomography of wide-angle obs data - Strategies for preconditioning and inversion. *Geophysical Journal International*, *192*(2), 1250–1280. https://doi.org/10.1093/gji/ggt165

Klingelhöfer, F., Edwards, R. A., Hobbs, R. W., & England, R. W. (2005). Crustal structure of the NE Rockall trough from wide-angle seismic data modeling. *Journal of Geophysical Research*, *110*(B11). https://doi.org/10.1029/2005jb003763

Kopp, H., Klaeschen, D., Flueh, E. R., Bialas, J., & Reichert, C. (2002). Crustal structure of the Java margin from seismic wide-angle and multichannel reflection data. *Journal of Geophysical Research*, *107*(B2). https://doi.org/10.1029/2000jb000095

Krampe, V., Edme, P., & Maurer, H. (2020). Optimized experimental design for seismic full waveform inversion: A computationally efficient method including a flexible implementation of acquisition costs. *Geophysical Prospecting*, *69*(1), 152–166. https://doi.org/10.1111/1365-2478.13040

Li, D., & Harris, J. M. (2018). Full waveform inversion with nonlocal similarity and model-derivative domain adaptive sparsity-promoting regularization. *Geophysical Journal International*, *215*(3), 1841–1864. https://doi.org/10.1093/gji/ggy380

Li, H., Li, J., Luo, S., Bem, T. S., Yao, H., & Huang, X. (2023). Continent-continent collision between the south and north China plates revealed by seismic refraction and reflection at the southern segment of the Tanlu fault zone. *Journal of Geophysical Research: Solid Earth*, *128*(1). https://doi.org/10.1029/2022jb025748

Maurer, H., Nuber, A., Martiartu, N. K., Reiser, F., Boehm, C., Manukyan, E., et al. (2017). Optimized experimental design in the context of seismic full waveform inversion and seismic waveform imaging. *Advances in Geophysics*, 1–45. https://doi.org/10.1016/bs.agph.2017.10.001

McGeary, S., & Warner, M. R. (1985). Seismic profiling the continental lithosphere. *Nature*, *317*(6040), 795–797. https://doi.org/10.1038/317795a0

Miller, D., Oristaglio, M., & Beylkin, G. (1987). A new slant on seismic imaging: Migration and integral geometry. *Geophysics*, *52*(7), 943–964. https://doi.org/10.1190/1.1442364

Minshull, T. A., Singh, S. C., & Westbrook, G. K. (1994). Seismic velocity structure at a gas hydrate reflector, offshore western Colombia, from full waveform inversion. *Journal of Geophysical Research*, *99*(B3), 4715–4734. https://doi.org/10.1029/93jb03282

Monk, D. (2020). Survey design and seismic acquisition for land, marine, and in-between in light of new technology and techniques. *Society of Exploration Geophysicists*. https://doi.org/10.1190/1.9781560803713

Morgan, J., Warner, M., Arnoux, G., Hooft, E., Toomey, D., VanderBeek, B., & Wilcock, W. (2016). Next-generation seismic experiments – II: Wide-angle, multi-azimuth, 3-D, full-waveform inversion of sparse field data. *Geophysical Journal International*, *204*(2), 1342–1363. https://doi.org/10.1093/gji/ggv513

Morgan, J., Warner, M., Bell, R., Ashley, J., Barnes, D., Little, R., et al. (2013). Next-generation seismic experiments: Wide-angle, multi-azimuth, three-dimensional, full-waveform inversion. *Geophysical Journal International*, *195*(3), 1657–1678. https://doi.org/10.1093/gji/ggt345

Métivier, L., & Brossier, R. (2016). The SEISCOPE optimization toolbox: A large-scale nonlinear optimization library based on reverse communication. *Geophysics*, *81*(2), F11–F25. https://doi.org/10.1190/geo2015-0031.1

Métivier, L., Brossier, R., Mérigot, Q., & Oudet, E. (2019). A graph space optimal transport distance as a generalization of L^p distances: Application to a seismic imaging inverse problem. *Inverse Problems*, *35*(8), 085001. https://doi.org/10.1088/1361-6420/ab206f

Nocedal, J., & Wright, S. J. (2006). *Numerical optimization* (2nd ed.). Springer.

Operto, S., Amestoy, P., Aghamiry, H., Beller, S., Buttari, A., Combe, L., et al. (2023). Is 3D frequency-domain FWI of full-azimuth/long-offset OBN data feasible? The gorgon data FWI case study. *The Leading Edge*, *42*(3), 173–183. https://doi.org/10.1190/tle42030173.1

Operto, S., Virieux, J., Dessa, J. X., & Pascal, G. (2006). Crustal imaging from multifold ocean bottom seismometers data by frequency-domain full-waveform tomography: Application to the eastern nankai trough. *Journal of Geophysical Research*, *111*(B09306). https://doi.org/10.1029/2005JB003835

Plessix, R. E. (2006). A review of the adjoint-state method for computing the gradient of a functional with geophysical applications. *Geophysical Journal International*, *167*(2), 495–503. https://doi.org/10.1111/j.1365-246x.2006.02978.x

Ravaut, C., Operto, S., Improta, L., Virieux, J., Herrero, A., & dell'Aversana, P. (2004). Multi-scale imaging of complex structures from multi-fold wide-aperture seismic data by frequency-domain full-wavefield inversions: Application to a thrust belt. *Geophysical Journal International*, *159*(3), 1032–1056. https://doi.org/10.1111/j.1365-246x.2004.02442.x

Sambolian, S., Brossier, R., & Métivier, L. (2022). *Exploiting the richness of multi-component data: A time-Dependent polarization-based Fwi approach. In 83rd EAGE annual conference and exhibition*. European Association of Geoscientists & Engineers. https://doi.org/10.3997/2214-4609.202210482

Schultz, A. P., & Crosson, R. S. (1996). Seismic velocity structure across the central Washington Cascade Range from refraction interpretation with earthquake sources. *Journal of Geophysical Research*, *101*(B12), 27899–27915. https://doi.org/10.1029/96jb02289

Sedova, A., Royle, G., Allemand, T., Lambaré, G., & Hermant, O. (2019). High-frequency acoustic land full-waveform inversion: A case study from the Sultanate of Oman. *First Break*, *37*(1), 75–81. https://doi.org/10.3997/1365-2397.n0010

Shin, C., Yoon, K., Marfurt, K. J., Park, K., Yang, D., Lim, H. Y., et al. (2001). Efficient calculation of a partial derivative wavefield using reciprocity for seismic imaging and inversion. *Geophysics*, *66*(6), 1856–1863. https://doi.org/10.1190/1.1487129

Stern, T., & Benson, A. (2011). Wide-angle seismic imaging beneath an andesitic arc: Central North Island, New Zealand. *Journal of Geophysical Research*, *116*(B9), B09308. https://doi.org/10.1029/2011jb008337

Tromp, J. (2019). Seismic wavefield imaging of earth's interior across scales. *Nature Reviews Earth & Environment*, *1*, 1–14. https://doi.org/10.1038/s43017-019-0003-8

Van Avendonk, H. J. A., Holbrook, W. S., Nunes, G. T., Shillington, D. J., Tucholke, B. E., Louden, K. E., et al. (2006). Seismic velocity structure of the rifted margin of the eastern Grand Banks of Newfoundland, Canada. *Journal of Geophysical Research*, *111*(B11). https://doi.org/10.1029/2005jb004156

Vermeer, G. J. O. (2003). 3D seismic survey design optimization. *The Leading Edge*, *22*(10), 934–941. https://doi.org/10.1190/1.1623633

Vermeer, G. J. O. (2012). *8. Factors affecting spatial resolution. In 3D seismic survey design* (2nd ed., pp. 247–262). Society of Exploration Geophysicists. https://doi.org/10.1190/1.9781560803041.ch8

Virieux, J., & Operto, S. (2009). An overview of full waveform inversion in exploration geophysics. *Geophysics*, *74*(6), WCC1–WCC26. https://doi.org/10.1190/1.3238367

Wu, S., Verschuur, D. J., & Blacquiere, G. (2022). Automated seismic acquisition geometry design for optimized illumination at the target: A linearized approach. *IEEE Transactions on Geoscience and Remote Sensing*, *60*, 1–13. https://doi.org/10.1109/tgrs.2021.3131365

Yang, P., Brossier, R., Métivier, L., Virieux, J., & Zhou, W. (2018). A time-domain preconditioned truncated Newton approach to multiparameter visco-acoustic full waveform inversion. *SIAM Journal on Scientific Computing*, *40*(4), B1101–B1130. https://doi.org/10.1137/17M1126126

Yang, Q., Zhou, B., Riahi, M. K., & Al-Khaleel, M. (2021). Frequency-domain seismic data transformation from point source to line source for 2D viscoelastic anisotropic media. *GEOPHYSICS*, *87*(2), T85–T98. https://doi.org/10.1190/geo2021-0166.1

Zand, T., & Górszczyk, A. (2024). Integrated algorithm for high-resolution crustal-scale imaging using complementary OBS and streamer data. *Earth and Space Science*, *11*(2). https://doi.org/10.1029/2023ea003264

Zeng, C., Dong, S., & Wang, B. (2014). Least-squares reverse time migration: Inversion-based imaging toward true reflectivity. *The Leading Edge*, *33*(9), 962–968. https://doi.org/10.1190/tle33090962.1

Zhou, H.-W., Hu, H., Zou, Z., Wo, Y., & Youn, O. (2018). Reverse time migration: A prospect of seismic imaging methodology. *Earth-Science Reviews*, *179*, 207–227. https://doi.org/10.1016/j.earscirev.2018.02.008

Zhu, L., Liu, E., & McClellan, J. H. (2017). Sparse-promoting full-waveform inversion based on online orthonormal dictionary learning. *Geophysics*, *82*(2), R87–R107. https://doi.org/10.1190/geo2015-0632.1

References From the Supporting Information

Zelt, C., & Barton, P. J. (1998). Three-dimensional seismic refraction tomography: A comparison of two methods applied to data from the Faeroe basin. *Journal of Geophysical Research*, *103*(B4), 7187–7210.